Supplementary Information for "Coevolving edge rounding and shape of glacial erratics; the case of Shap granite, UK"

Paul A. Carling

1 Supplementary Method

1.1 Spallation

Loss of small fragments occurs on the block surface and can disrupt edge rounding locally, leaving scars, but such losses are difficult to parameterize (Olsen, 1983) and rarely have been addressed. Spallation was estimated by enumerating the number of sharp-edged scars on the exposed surfaces of the edges and faces of each individual block, to give *c*., 38 values for each location. Although an element of subjectivity is involved, using the same procedure and only one operator should demonstrate any significant differences in block populations.

1.2 Block shape

Shap granite blocks (L > 1m) were located in the field and the location recorded using a handheld Garmin gps. Locations sampled include Wasdale Bridge, Green Brow and sites in and around Teesdale, respectively 0.5km, 3.5km and 36-54km eastwards from the Wasdale Crag outcrop (Table S1). As the distance from the source outcrop increased the sampling area necessarily had to increase as the concentration of erratics became more dilute. Examples were selected that were sitting on exposed bedrock so as not to be partially buried. To obtain an indication of the size of the block and its overall shape, the lengths of the three orthogonal axes: long axis (L); medium axis (M) and the short axis (S) were recorded using a taut tape measure. In addition, a data set for the shape of Shap granite blocks

Table S1: General sampling locations

Location	Wasdale Old Bridge	Haybanks	Blasterfield	Goldsborough	Hunder Beck	Barnard Castle	Levy Pool
Northing	54.468994	54.484814	54.497372	54.554919	54.54376	54.546631	54.534203
Westing	2.673856	2.638158	2.565614	2.073394	2.1274	1.934722	2.051856

obtained from across the region, rather than along the easterly transect were available (Carling *et al*., 2023) to augment the transect data. Block shape can be described in terms of the degree of similarity to an oblong for sharp-edged blocks and to ellipsoids for more rounded blocks. In either case, the axes ($L > M > S$) or the semi-axes ($Lr > Mr > Sr$) can be used to define the volume of the oblong or ellipsoid. Oblongs and ellipsoids can be prolate to resemble blades and rods or oblate to resemble plates depending on the values of L, M and S. Cubes or spheres occur when $L = M = S$.

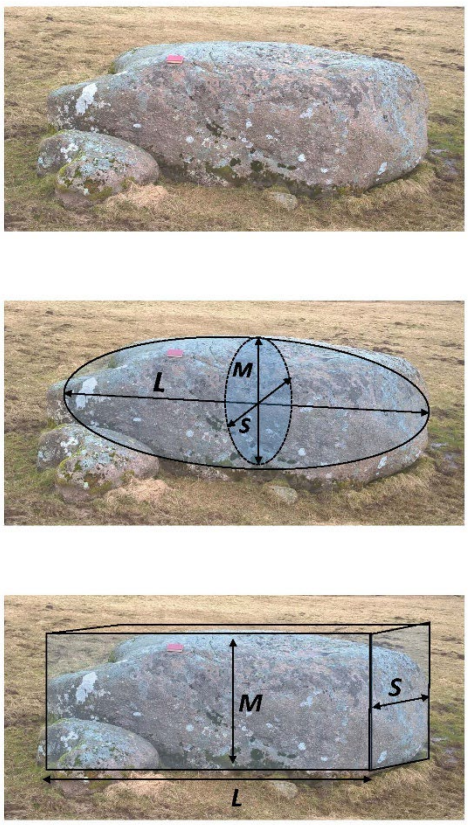

Figure S1: Simplified representations of Shap granite boulder shapes. A) Boulder in situ; B) Approximation based on inner fitting ellipsoid; C) Prismatic approximation based on bounding cuboid.

There are various means to describe block shapes and to display such data graphically (*e.g.*, Benn & Ballantyne, 1995; Oakey *et al*., 2005). In the main text I report the shape indices of Zingg (1935) and use the Zingg projection for its simplicity as data plotted therein show the lack of shape trends clearly. I also considered the Sneed and Folk (1958) shape descriptors, but I did not use their ternary diagram, as the limit points of blades and rods on a Sneed and Folk diagram are so similar as to be indistinguishable. Rather, here in the Supplement I make use of a simple ternary diagram (Hofmann, 1994) relating the readily understandable values of: *L*, *M* and *S*. Once normalized, the values of the axes (*L* > *M* > *S*) can be projected in a ternary diagram to illustrate the shape deviation of each block from the equant shape of a cube or a sphere.

As block shape is defined by the three axes, it would be preferable for graphical plotting if the three parameters could be reduced to two.

Normalization (*N*): $N_L = L/(L + M + S)$

$N_M = M/(L + M + S)$

$N_S = S/(L + M + S)$

Projections: $X = 0.5N_L + N_s$

$$Y = N_L(COS(30\pi)180)$$

This preference involved recalculating the values of L , M and S to sum to unity. In this manner the shape of each block can be defined as a vector having value and direction (Fig. S2).

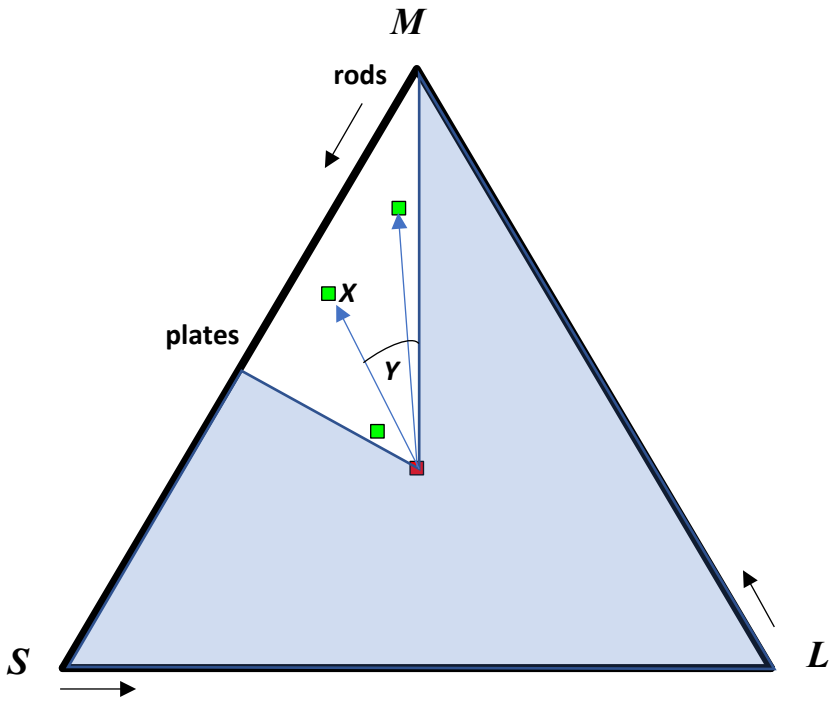

Figure S2: Plot similar to Hofmann (1994), used to define block shape. The normalized values of the semi-axes of three hypothetical blocks (rod, plate, cuboid) are plotted where the value X represents the distance from the centre of the plot where the red symbol represents a sphere. The value Y is equivalent to the angle from the vertical extending from the red symbol to the top vertex. The blue shaded area represents the region in which data cannot exist, give the rule: L > M > S.

Using this method, which is essentially similar to that of Hofmann (1994), the shape of each block readily can be plotted using the two values (*X*, *Y*), with blocks deviating from the equant shape of a cube or a sphere with distance away from the centre of the plot. As the distance (*X*) increases, the block becomes more rod-like but as the angular deviation (*Y*) increases away from the vertex the blocks become more plate-like. Blocks with small values of *X* are close to cuboids or spheres.

1.3 Edge rounding

Edge rounding was measured after Wentworth (1923). Where rounded edges were delimited by neighbouring flat facets, the three most prominent rounded edges, delimited by flat facets to either side, were identified by inspection. Two stainless steel straight edges joined by a pivot were used to locate the flat facets either side of the rounded edge (Fig. S3A). A coloured pencil was used to draw a straight line on the block in the plane A, B, C between the intersection points of the two straight planes

and the rounded edge. A flexible drafting curve was fitted to the surface of the block between the intersection points (Fig. S3A). In the field, the form of the curve was traced on a sheet of A4 or A3 paper secured to a clipboard. In the office, the rounded segment was defined by a straight line (*l*) drawn to join the ends of each curve and this length was recorded. The maximum height (*h*) of the segment was recorded at a right angle to the line, *l* (Fig. S3). The radius of curvature (r_c) of the inscribed circle within the rounded edge was then determined:

$$r_c = \frac{l^2}{8h} + \frac{h}{2} \qquad \text{(S1)}$$

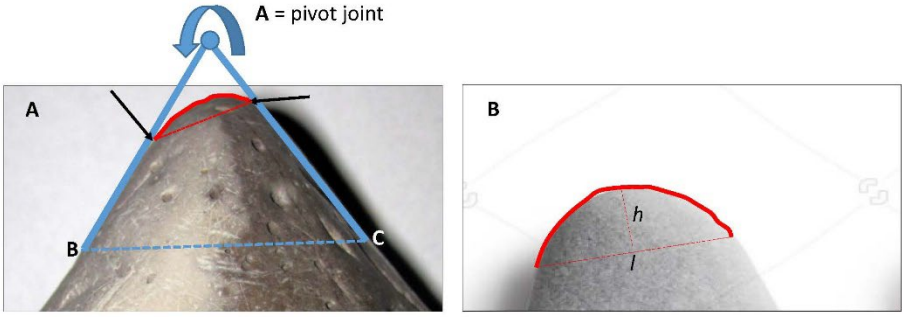

Figure S3: Method used to determine edge rounding in the field. A) Method used for edge rounding arcs, between straight facets. Arrows indicate the intersection points of the curved block surface and constraining straight edges; B) Definition of the method used to define the arc length (l) and the segment height (h). See text for detail.

Silver ratio block edge rounding model

A conceptual model of block rounding

An initial (parent) cube, fracturing across the *L*-axis, fractures to form two oblongs (Fig. S4A). These initial two oblongs each have two equal lengths, so either of these *M*-axes can be selected for further fracture. The subsequent two blocks are oblongs with three unequal lengths each and so there is only one *M*-axis to be selected for fracture. A further third fracture produces two cubes. Thus, four cubes appear after each third fracture in the series. Following this sequence, the initial 12 edges of the initial block reduce to give maximum values of 8, 5, 3, 1 and 0 edges with the initial parent characteristics after each subsequent fracture. The series 12 to 3 can be described by a quadratic equation but this cannot be extended to the 1 and 0 values due to the geometric constraints of the fracture sequence (Fig. S4B). Importantly, blocks with no initial parent edges preserved occur after five fracture events (Fig. S4C).

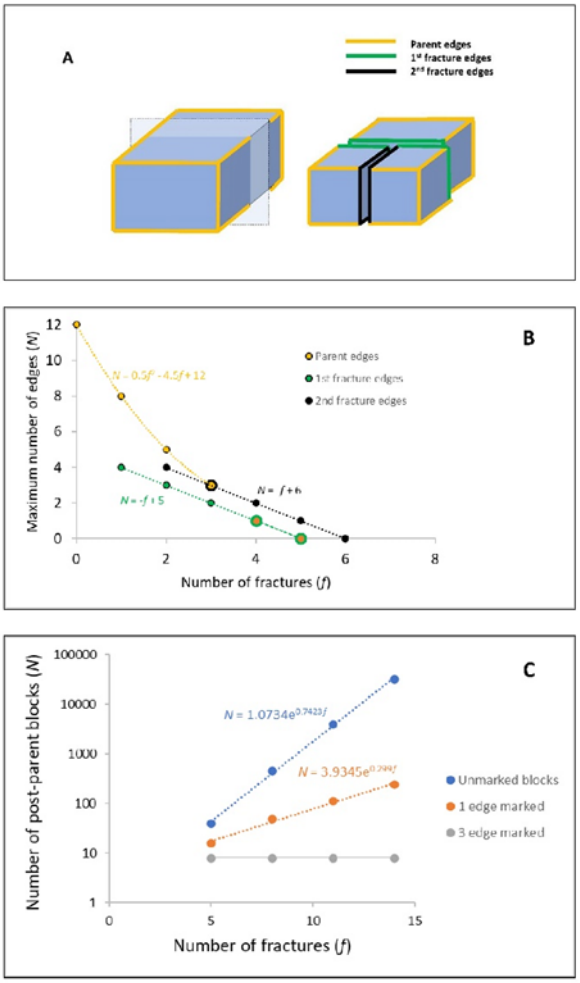

Figure S4: A) A regular block released from outcrop has 12 initial edges (Parent edges) all equally rounded. Fracturing the block at right angles (silver model) introduces four new edges (1st fracture edges) to each of two sibling blocks, which edges are younger than the initial edges. A further fracture is indicated by 2nd fracture edges; B) The maximum number of edges on a block as a function of the number of fracture events, with only the parent edges and those edges related to the first two fracture events plotted; C) The total number of blocks created at each fracture event which retain 0, 1 or 3 of the original parent edges.

The first fracture produces four new edges (to each sibling block), and subsequent fractures reduce these as an arithmetic linear progression: 4, 3, 2, 1 and 0 (Fig. S4B). Each subsequent fracture introduces a new set of four fracture edges which also follow an arithmetic linear progression.

Blocks reduced to display only one initial parent edge can be split to form two blocks, either: A) both having one initial edge, or B) one with an initial edge and one without. Beyond five fractures, the number of blocks displaying no initial edges increases exponentially, more rapidly than the number showing only one edge (Fig. S4C). In principle, four residual blocks will always display three initial edges, but these rapidly become statistically unimportant within the larger population. In the case of cubes, relaxing the rule that the next fracture is at a right angle to the prior fracture (whilst still maintaining blocks of equal mass upon division), three possible orthogonal fracture planes are possible, which is like the stochastic fracture model. When compared to extinction using the rule that fracture is across the *L*-axis, this latter model (not illustrated) can delay the extinction of any edge generation typically by only one or two fracture events.

Treatment of an erratic block as a stationary cuboid subject to flexure failure beneath moving ice

Treating the block as a rectangular body subject to potential bending leading to fracture, the average longitudinal shear force acting on a block with transverse breadth (*L*) and length (*M*) is given simply as:

$$\tau_{av} = \frac{V}{A}, \qquad \text{(S2)}$$

where *V* is the applied shear force and *A* = *L***M* is the area of the block subject to the tangential force of the moving ice. Taking a block with *L* = 2m and *M* = 2m, the on-line calculator for beam forces (Shear Stress Calculator (Beam Analysis); omnicalculator.com) indicates that a shear force of 22 MPa will impose a maximum shear stress τ_{max} at the point of fracture of 8.25 MPa. The peak force (τ_{max}) varies as the ratio of the two axes (*L*, *M*) are varied. For *L* = 3, *M* = 1, the peak force can be *c*., 1.73 times the average force such that the peak value of 8.25MPa might be achieved when the applied average force is 4.77MPa. Using the shear force values associated with these stress values in Eq. 2, the typical ice thickness ranges from 130m to 180m. Such values are generalizations for illustrative purposes and more complex geometries associated with ellipsoidal erratics would yield somewhat different results.

2 Supplementary Results

2.1 Spallation

Spallation was more evident closer to the source. At Wasdale Old Bridge, only 0.8km from the outcrop, block faces often visually were rugose, even if distinct spallation points were not evident. Spallation on edges was more readily identified than spallation sites on faces. In contrast, with distance from the source, block surfaces tended to exhibit visually smoothed curved surfaces, lacking spallation. Shallow dished scoops occur at distance (from Haybanks eastwards) where spallation points have been smoothed but not removed.

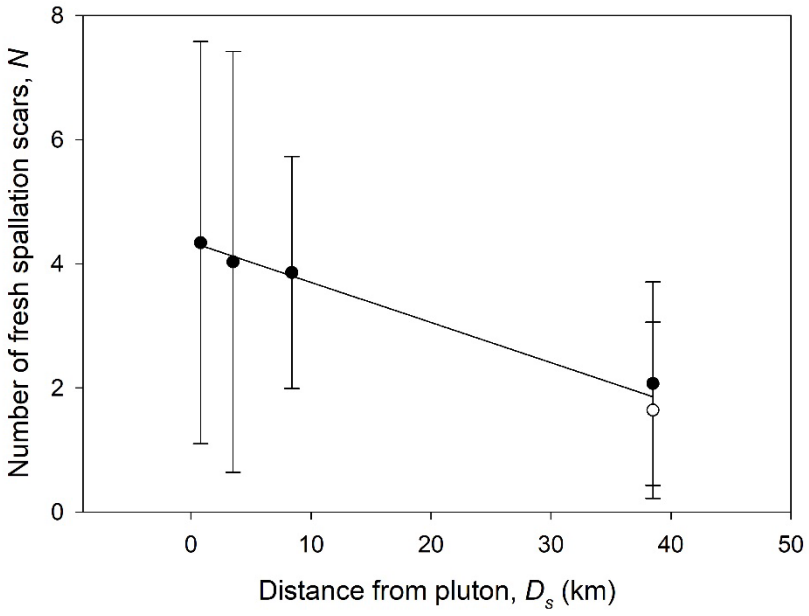

Figure S5: Linear trend in the reduction in the number (N) of fresh spallation scars with distance (D_s) from the pluton. At c., 38km scars become more difficult to define, so a maximum estimate (closed symbol) and minimum estimate (open symbol) are included. Error bars are ± 1 standard deviation. Thirty-eight data points in each case, except at 38.5km where the number is 33.

Spallation scars are more prevalent close to the outcrop, where edges are sharp and faces rugose, and are less frequently observed on the smooth rounded block surfaces distal from the outcrop (Fig. S5). Such a negative linear trend in spallation relates to a reduction with distance in the presence of excrescences or microstructural defects, both on edges and on the faces subject to critical ice-loading pressure. Structural failure along a short arc within the excrescent rock mass is more likely than across greater lengths within the block as microstructural defects lead to the propagation of localized fracture (Li *et al*., 2020; Guo *et al*., 2023) until such excrescences are removed. With increased distance from the pluton, there are fewer excrescences and edges are more rounded, so spallation is less frequent and those scars that already exist are abraded smooth. Consequently, spallation is a process that diminishes with distance and is worthy of closer investigation. The present study did not consider the size of spallation scars and a future study might utilize laser scanning to obtain quantitative mass loss data, as the role of spallation in block size reduction has been neglected.

2.2 Block shape

The normalised shapes of blocks are shown in ternary diagrams (Fig. S6). Within Fig. S6A & B, the central triple point is the only location where perfect cubes and spheres can exist. The Wasdale Old Bridge blocks (Fig. S6A), less than 0.8km from the source outcrop, plot close to the triple point, being cubic in form. Yet, many blocks distal from the source (Fig. S6B) still display fairly equant forms. The two green squares, joined by a straight black line represent the arbitrarily selected shape ratios: 3:1:1 and 3:3:1 above which 'limit' more rod-like and plate-like ellipsoid forms occur, albeit scarcely. These results indicates that rod-like and plate-like forms are mechanically unstable, and blocks break down preferentially towards equant forms, which progression indicates that 'parent' blocks, released at the pluton outcrop, tend to spawn 'children' of similar form, which issue is considered next.

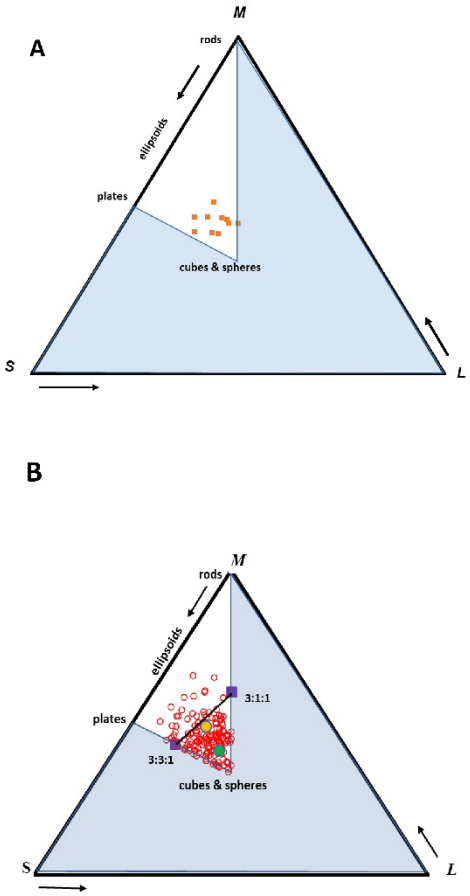

Figure S6: Normalized block axes (values > 0 to < 1) displayed within a Hoffman (1994; 1995) ternary diagram to define block shapes. Given the inequality: L > M > S no data can plot within the shaded portion of the figure. A) Blocks near Wasdale Old Bridge, 0.8km from the source outcrop, cluster close to equant shapes with no examples of prolate (rod) or oblate (plate) forms (n = 28; several coincident points); B) Blocks, 10's of km from source, sampled from across the system show a broader range of shapes, including a few more plate-like and rod-like forms (n = 151). Gold and green symbols are the system state attractors for the fracture model and the silver model respectively (see main text).

References

Benn, D.I., Ballantyne, C.K.: Grain-shape indices and isometric graphs — Discussion. *Journal of Sedimentary Research*, A65, 719-721, https://doi.org/10.1306/D42681C6-2B26-11D7-8648000102C1865D, 1995.

Guo, P., Zhang, P., Bu, M, Wang, J., Zheng, X., He, M.: Microcracking behavior and damage mechanisms of granite subject to high temperature based on CT-GBM numerical simulation. *Computers and Geotechnics*, 159, 105385, https://doi.org/10.1016/j.compgeo.2023.105385, 2023.

Hofmann, H.J.: Grain-shape indices and isometric graphs. *Journal of Sedimentary Research*, A64, 916-920, https://doi.org/10.1306/D4267F0A-2B26-11D7-8648000102C1865D, 1994.

Hofmann, H.J.: Grain-shape indices and isometric graphs — Reply. *Journal of Sedimentary Research*, A65, 721-723, https://doi.org/10.1306/D42681C6-2B26-11D7-8648000102C1865D, 1995.

Oakey, R.J., Green, M., Carling, P.A., Lee, M.W.E., Sear, D.A., Warburton, J.: Grain-shape analysis– A new method for determining representative blocks shapes for populations of natural grains. *Journal of Sedimentary Research*, 75, 1065-1073, https://doi.org/10.2110/jsr.2005.079, 2005.

Olsen, L.: A method for determining total block roundness in sediments. *Boreas*, 12, 17-21, http://dx.doi.org/10.1111/j.1502-3885.1983.tb00355.x, 1983.

Sneed, E.D., Folk, R.L.: Pebbles in the lower Colorado River, Texas — A study of blocks morphogenesis. *Journal of Geology*, 66, 114-150, 1958.

Wentworth, C.K.: A method of measuring and plotting the shapes of pebbles. *US Geological Society Bulletin* 730-C, 91-102. doi: 10.3133/B730C, 1923.

Zingg, T.: Beitrag zur schotteranalyse. PhD thesis, ETH Zurich, 1935.